Quantum kinetics of quenched two-dimensional Bose superfluids

Clément Duval* and Nicolas Cherroret†
Laboratoire Kastler Brossel, Sorbonne Université, CNRS, ENS-PSL Research University, Collège de France, 4 Place Jussieu, 75005 Paris, France

(Received 21 February 2023; accepted 23 March 2023; published 6 April 2023)

We study theoretically the nonequilibrium dynamics of a two-dimensional (2D) uniform Bose superfluid following a quantum quench, from its short-time (prethermal) coherent dynamics to its long-time thermalization. Using a quantum hydrodynamic description combined with a Keldysh field formalism, we derive quantum kinetic equations for the low-energy phononic excitations of the system and characterize both their normal and anomalous momentum distributions. We apply this formalism to the interaction quench of a 2D Bose gas and study the ensuing dynamics of its quantum structure factor and coherence function, both recently measured experimentally. Our results indicate that, in two dimensions, a description in terms of independent quasiparticles becomes quickly inaccurate and should be systematically questioned when dealing with nonequilibrium scenarios.

DOI: 10.1103/PhysRevA.107.043305

I. INTRODUCTION

The out-of-equilibrium dynamics of isolated quantum many-body systems revealed a rich panel of scenarios in the recent years. In the generic case of ergodic systems, the Eigenstate Thermalization Hypothesis is expected to hold, such that at sufficiently long time any local observable acquires a value taken from a Gibbs ensemble [1,2]. In the context of experiments on cold-atomic gases, the relaxation dynamics following a quantum quench has been especially explored in one dimension, both in the weakly [3,4] and strongly [5,6] interacting regimes. In the latter case, interesting theoretical predictions were also made using nonquadratic Luttinger-liquid models [7–10], such as an algebraic relaxation toward equilibrium [9,11]. In parallel, the peculiar case of systems escaping thermalization attracted much attention in connection with integrability [12,13] or many-body localization [14–16].

In higher dimensions, a new generation of experiments has recently appeared, exploring, e.g., the relaxation dynamics of cold-atomic gases in the strong-interaction limit [17,18] or the emergence of universal scaling laws in the vicinity of the condensation transition in three dimensions [19,20]. Concomitantly, theoretical developments based on quantum kinetic approaches were proposed to describe the nonequilibrium evolution of three-dimensional (3D) isolated quantum gases toward thermalization [21–24]. In comparison, on the other hand, two-dimensional (2D) nonequilibrium Bose gases have so far received less attention. Different from 3D Bose gases, only superfluid quasicondensates with algebraic long-range order exist for ultracold bosons in two dimensions, which requires a special treatment of phase fluctuations [25–27]. Two-dimensional Bose gases also experience an interaction-driven Kosterlitz-Thouless transition, around which the dynamics exhibits specific temporal features [28–30]. Generally speaking, the ability to restrict the atomic motion to two dimensions using confining optical potentials has allowed for more and more accurate experiments of nonequilibrium physics with quantum fluids [30–32]. In the context of optics, finally, a number of experiments involving "fluids of light" [33,34] have emerged, in particular in cavity-less, nonlinear materials where the propagation of a laser mimics the out-of-equilibrium dynamics of 2D dilute ultracold Bose gases undergoing an interaction quench [35–39].

In this paper, we present a theoretical description of the nonequilibrium quantum evolution of 2D, isolated uniform Bose superfluids following a quantum quench, which captures both the short timescales, where the dynamics is fully coherent, and the long timescales, where thermalization occurs. To this aim, we develop a quantum kinetic formalism describing interactions between the low-lying phononic excitations of the superfluid, combining a quantum hydrodynamic representation with a Keldysh field formalism. This allows us to go beyond recent theoretical developments based on independent quasiparticles and therefore restricted to short evolution times after the quench [40–45]. Within our approach, we derive kinetic equations for both the normal and anomalous momentum distributions of the phonons, which, unlike the equilibrium Bose gases, are both needed to faithfully capture the nonequilibrium evolution [9,22]. Close to equilibrium, in particular, we recover the Landau and Beliaev scattering rates associated with three-phonon interaction processes [46–49]. We finally apply this formalism to a concrete example, a quench of the interaction strength in a 2D superfluid, and analyze the subsequent time evolution of the structure factor and of the spatial coherence function, recently measured in cold-atom [31] and optical-fluid [38,39] experiments. Our approach, in particular, includes recent developments [42] allowing for a proper treatment of the finite quench duration,

*clement.duval@lkb.upmc.fr
†nicolas.cherroret@lkb.upmc.fr

crucial to avoid the unphysical divergences of the postquench superfluid's energy.

The article is organized as follows. In Sec. II, we introduce the quantum hydrodynamic description of 2D superfluids and construct the nonequilibrium interacting Keldysh action in the basis of independent quasiparticles. Section III presents the technical details on the field and perturbation theories, as well as a derivation of kinetic equations for the normal and anomalous phonon distributions. The kinetic equations and their near-equilibrium properties are discussed in Sec. IV. In Sec. V, we apply our formalism to the calculation of the time evolution of the nonequilibrium structure factor and the coherence function of a 2D Bose gas following an interaction quench. Section VI finally concludes the article.

II. HYDRODYNAMIC FORMULATION

A. Hydrodynamic Hamiltonian

Our starting point is the many-body Hamiltonian of a uniform, low-temperature, 2D gas of bosons with repulsive contact interactions:

$$\hat{H} = \int d^2\boldsymbol{r}\left(-\frac{1}{2m}\hat{\psi}^\dagger\Delta_{\boldsymbol{r}}\hat{\psi} + \frac{g}{2}\hat{\psi}^\dagger\hat{\psi}^\dagger\hat{\psi}\hat{\psi}\right), \tag{1}$$

where the field operators $\hat{\psi}$ satisfy the bosonic canonical commutation rule $[\hat{\psi}(\boldsymbol{r}), \hat{\psi}^\dagger(\boldsymbol{r}')] = \delta(\boldsymbol{r}-\boldsymbol{r}')$ and we set $\hbar = 1$. In low dimensions, collective excitations of the Bose gas are most conveniently described within a quantum hydrodynamic formalism, where the field operator is expressed in the density-phase representation [27,50]:

$$\hat{\psi}(\boldsymbol{r}) = e^{i\hat{\theta}(\boldsymbol{r})}\sqrt{\hat{\rho}(\boldsymbol{r})}, \tag{2}$$

with the commutation rule $[\hat{\rho}(\boldsymbol{r}), \hat{\theta}(\boldsymbol{r}')] = i\delta(\boldsymbol{r}-\boldsymbol{r}')$. At low temperature, phase fluctuations of the 2D Bose gas are generally not small, in contrast to density fluctuations and phase gradients [25–27]. By writing $\hat{\rho}(\boldsymbol{r}) = \rho_0 + \delta\hat{\rho}(\boldsymbol{r})$ with ρ_0 the mean gas density, we can then expand the Hamiltonian (1) with respect to $\delta\hat{\rho}$ and $\nabla_{\boldsymbol{r}}\hat{\theta}$. This leads to [26,51,52]

$$\hat{H} = \int d\boldsymbol{r}\Bigg[\frac{\rho_0}{2m}(\nabla_{\boldsymbol{r}}\hat{\theta})^2 + \frac{g}{2}(\delta\hat{\rho})^2 + \frac{1}{8m\rho_0}(\nabla_{\boldsymbol{r}}\delta\hat{\rho})^2 + \frac{1}{2m}(\nabla_{\boldsymbol{r}}\hat{\theta})\delta\hat{\rho}(\nabla_{\boldsymbol{r}}\hat{\theta})\Bigg], \tag{3}$$

where we redefined the energy scale $\hat{H} \to \hat{H} - g\rho_0/2$ and dropped a cubic term $\propto (\nabla_{\boldsymbol{r}}\delta\hat{\rho})^2\delta\hat{\rho}$, negligible at low energy [26,51].

B. Bogoliubov transformation

The Hamiltonian (3) is the sum of a quadratic part $\hat{H}_0$ and a cubic interaction term $\hat{H}_{\rm int}$. The quadratic part is nondiagonal, but is customarily diagonalized by means of a Bogoliubov transformation [53]. To proceed, we first rewrite Eq. (3) in momentum space, introducing the Fourier variables

$$\hat{\theta}_{\boldsymbol{q}} \equiv \rho_0\int d\boldsymbol{r}e^{-i\boldsymbol{q}\cdot\boldsymbol{r}}\hat{\theta}(\boldsymbol{r}), \quad \delta\hat{\rho}_{\boldsymbol{q}} \equiv \int d\boldsymbol{r}e^{-i\boldsymbol{q}\cdot\boldsymbol{r}}\delta\hat{\rho}(\boldsymbol{r}). \tag{4}$$

The quadratic part of the Hamiltonian becomes

$$\hat{H}_0 = \int_{\boldsymbol{q}}\left[\frac{q^2}{2m}\hat{\theta}_{\boldsymbol{q}}\hat{\theta}_{-\boldsymbol{q}} + \left(\frac{g\rho_0}{2} + \frac{q^2}{8m}\right)\delta\hat{\rho}_{\boldsymbol{q}}\delta\hat{\rho}_{-\boldsymbol{q}}\right], \tag{5}$$

where we introduced the short-hand notation $\int_{\boldsymbol{q}} \equiv \int d^2\boldsymbol{q}/[(2\pi)^2\rho_0]$. To diagonalize $\hat{H}_0$, we introduce new operators $\hat{a}_{\boldsymbol{q}}$ and $\hat{a}^\dagger_{\boldsymbol{q}}$, defined through the Bogoliubov transformation

$$\delta\hat{\rho}_{\boldsymbol{q}} = -\sqrt{\frac{E_{\boldsymbol{q}}}{\epsilon_{\boldsymbol{q}}}}(\hat{a}^\dagger_{\boldsymbol{q}} + \hat{a}_{-\boldsymbol{q}}), \tag{6}$$

$$\hat{\theta}_{\boldsymbol{q}} = \frac{i}{2}\sqrt{\frac{\epsilon_{\boldsymbol{q}}}{E_{\boldsymbol{q}}}}(\hat{a}^\dagger_{\boldsymbol{q}} - \hat{a}_{-\boldsymbol{q}}), \tag{7}$$

where $E_{\boldsymbol{q}} \equiv \boldsymbol{q}^2/(2m)$ and $\epsilon_{\boldsymbol{q}} \equiv \sqrt{E_{\boldsymbol{q}}(E_{\boldsymbol{q}} + 2g\rho_0)}$ is the well-known Bogoliubov dispersion relation. Inserting this basis change into Eq. (5), we obtain

$$\hat{H}_0 = \int_{\boldsymbol{q}}\epsilon_{\boldsymbol{q}}\left(\hat{a}^\dagger_{\boldsymbol{q}}\hat{a}_{\boldsymbol{q}} + \frac{1}{2}\right), \tag{8}$$

which describes a gas of free quasiparticles with energy dispersion $\epsilon_{\boldsymbol{q}}$. At momenta $|\boldsymbol{q}| \ll 1/\xi$, where $\xi \equiv \sqrt{1/4g\rho_0 m}$ is the healing length, the dispersion relation becomes phononic

$$\epsilon_{\boldsymbol{q}} \simeq c|\boldsymbol{q}|, \tag{9}$$

where $c = \sqrt{g\rho_0/m}$ is the speed of sound. Unless stated otherwise, in the rest of the paper we will mainly focus on the low-energy regime where Eq. (9) holds.

In terms of the Bogoliubov operators $\hat{a}_{\boldsymbol{q}}$ and $\hat{a}^\dagger_{\boldsymbol{q}}$, the interaction term in the hydrodynamic Hamiltonian (3) reads

$$\hat{H}_{\rm int} = \int_{\boldsymbol{p},\boldsymbol{q}}\Lambda_{\boldsymbol{p},\boldsymbol{q}}(\hat{a}_{\boldsymbol{p}}\hat{a}_{\boldsymbol{q}}\hat{a}^\dagger_{\boldsymbol{p}+\boldsymbol{q}} + \text{H.c.}), \tag{10}$$

where, in the phononic regime $|\boldsymbol{q}| \ll 1/\xi$, the vertex function $\Lambda_{\boldsymbol{p},\boldsymbol{q}}$ is given by

$$\Lambda_{\boldsymbol{p},\boldsymbol{q}} \simeq \frac{3}{4m}\sqrt{\frac{g\rho_0}{2c}}\sqrt{|\boldsymbol{p}|\,|\boldsymbol{q}|\,|\boldsymbol{p}+\boldsymbol{q}|}. \tag{11}$$

The cubic interaction (10) describes a three-phonon scattering process with momentum conservation. In two dimensions it can also be resonant, i.e., there exists a range of $\boldsymbol{p},\boldsymbol{q}$ values satisfying $\epsilon_{\boldsymbol{p}} + \epsilon_{\boldsymbol{q}} = \epsilon_{\boldsymbol{p}+\boldsymbol{q}}$ [9,54]. As will be shown in Sec. III C, this property leads to a divergence of the self-energy, which makes this process the dominant one for the dynamics. For this reason, when writing Eq. (10) we dropped the interaction terms of the type $\hat{a}_{\boldsymbol{p}}\hat{a}_{\boldsymbol{q}}\hat{a}_{-\boldsymbol{p}-\boldsymbol{q}}$, which cannot be resonant and are therefore subdominant.

C. Nonequilibrium action

In this work, we consider a 2D Bose gas initially described by an equilibrium density matrix $\hat{\rho}_0$, and we examine its subsequent dynamics following a quantum quench performed at $t = 0$. To this aim, from now on we work in the Heisenberg representation for operators (with, for instance, $\hat{a}_{\boldsymbol{q},t} = e^{i\hat{H}t}\hat{a}_{\boldsymbol{q},t=0}e^{-i\hat{H}t}$), and consider the time evolution of the phonon normal and anomalous momentum distributions,

defined as

$$n_{\boldsymbol{q},t} \equiv \langle \hat{a}^\dagger_{\boldsymbol{q},t} \hat{a}_{\boldsymbol{q},t} \rangle, \tag{12}$$

$$m_{\boldsymbol{q},t} \equiv |\langle \hat{a}_{\boldsymbol{q},t} \hat{a}_{-\boldsymbol{q},t} \rangle|, \tag{13}$$

where the quantum-mechanical average is performed over the initial density matrix: $\langle \ldots \rangle = \mathrm{Tr}(\hat{\rho}_0 \ldots)$.

When the interaction term (10) in the Hamiltonian is neglected, the Heisenberg equations of motion following from Eq. (8) lead to a purely harmonic evolution of the Bogoliubov operators, $\hat{a}_{\boldsymbol{q},t} = \hat{a}_{\boldsymbol{q},0} e^{-i\epsilon_q t}$, so that

$$n_{\boldsymbol{q},t} = n_{\boldsymbol{q},0} \quad m_{\boldsymbol{q},t} = m_{\boldsymbol{q},0}. \tag{14}$$

The normal and anomalous phonon momentum distributions thus remain stuck to their initial value (more precisely, to their postquench value, see Sec. V), as expected from a free-field theory.

To capture the time dependence of $n_{\boldsymbol{q},t}$ and $m_{\boldsymbol{q},t}$ pertained to the cubic interaction (10), we use the Keldysh field formalism [55,56], i.e., we replace the quantum mechanical averages (12) and (13) by path integrals on the closed-time contour $\mathcal{C} = \{\mathcal{C}_+, \mathcal{C}_-\}$ with the forward path $\mathcal{C}_+$ ranging from $t = 0$ to ∞ and the reversed path from ∞ to 0. This amounts to doubling the degrees the freedom, i.e., we work with two sets of scalar fields a_+, a_+^* and a_-, a_- and the partition function

$$\mathcal{Z} = \int \mathcal{D}[a_+, a_+^*, a_-, a_-^*] e^{iS(a_+, a_+^*) - iS(a_-, a_-^*)}, \tag{15}$$

where the hydrodynamic action in the coherent-state representation follows from Eqs. (8) and (10):

$$S(a, a^*) = S_0 + S_{\mathrm{int}} = \int_{\boldsymbol{q},t} a^*_{\boldsymbol{q},t} (i\partial_t - \epsilon_{\boldsymbol{q}}) a_{\boldsymbol{q},t} + \int_{\boldsymbol{p},\boldsymbol{q},t} \Lambda_{\boldsymbol{p},\boldsymbol{q}} (a_{\boldsymbol{p},t} a_{\boldsymbol{q},t} a^*_{\boldsymbol{p}+\boldsymbol{q},t} + \mathrm{c.c.}), \tag{16}$$

with the shorthand notation $\int_t = \int_{\mathcal{C}_\pm} dt$ for $a = a_\pm$. Both time integrals over $\mathcal{C}_+$ and $\mathcal{C}_-$ are conveniently reduced to a single integral over $t > 0$ by introducing the "classical" and "quantum" field variables $\alpha = (a_+ + a_-)/\sqrt{2}$ and $\tilde{\alpha} = (a_+ - a_-)/\sqrt{2}$ [53,57]. Under this transformation, the quadratic action becomes

$$S_0 = \int_{\boldsymbol{q},t>0} \begin{pmatrix} \alpha^*_{\boldsymbol{q},t} & \tilde{\alpha}^*_{\boldsymbol{q},t} \end{pmatrix} [\mathbf{G}^0]^{-1}_{\boldsymbol{q},t,t} \begin{pmatrix} \alpha_{\boldsymbol{q},t} \\ \tilde{\alpha}_{\boldsymbol{q},t} \end{pmatrix}, \tag{17}$$

where

$$[\mathbf{G}^0]^{-1}_{\boldsymbol{q},t,t} = \begin{pmatrix} 0 & i\partial_t - \epsilon_{\boldsymbol{q}} - i0^+ \\ i\partial_t - \epsilon_{\boldsymbol{q}} + i0^+ & 2i0^+(2n_{\boldsymbol{q},0} + 1) \end{pmatrix}, \tag{18}$$

while the interaction part is expressed as

$$S_{\mathrm{int}} = \frac{1}{\sqrt{2}} \int_{\boldsymbol{p},\boldsymbol{q},t>0} \Lambda_{\boldsymbol{p},\boldsymbol{q}} (2\alpha^*_{\boldsymbol{p}+\boldsymbol{q},t} \tilde{\alpha}_{\boldsymbol{p},t} \alpha_{\boldsymbol{q},t} + \tilde{\alpha}^*_{\boldsymbol{p}+\boldsymbol{q},t} \alpha_{\boldsymbol{p},t} \alpha_{\boldsymbol{q},t} + \tilde{\alpha}^*_{\boldsymbol{p}+\boldsymbol{q},t} \tilde{\alpha}_{\boldsymbol{p},t} \tilde{\alpha}_{\boldsymbol{q},t} + \mathrm{c.c.}). \tag{19}$$

The Keldysh actions (17) and (19) constitute the starting point of the nonequilibrium perturbation theory that is presented in the next section.

III. PERTUBATION THEORY

A. Quantum kinetic equation

To construct the perturbation theory, we introduce three fundamental correlators, the retarded G^R, advanced G^A, and Keldysh G^K Green's functions

$$G^R_{\boldsymbol{q},t,t'} \equiv -i\Theta(t - t') \langle [\hat{a}_{\boldsymbol{q},t}, \hat{a}^\dagger_{\boldsymbol{q},t'}] \rangle = -i \langle \alpha_{\boldsymbol{q},t} \tilde{\alpha}^*_{\boldsymbol{q},t'} \rangle, \tag{20}$$

$$G^A_{\boldsymbol{q},t,t'} \equiv i\Theta(t' - t) \langle [\hat{a}_{\boldsymbol{q},t}, \hat{a}^\dagger_{\boldsymbol{q},t'}] \rangle = -i \langle \tilde{\alpha}_{\boldsymbol{q},t} \alpha^*_{\boldsymbol{q},t'} \rangle, \tag{21}$$

$$G^K_{\boldsymbol{q},t,t'} \equiv -i \langle \{\hat{a}_{\boldsymbol{q},t}, \hat{a}^\dagger_{\boldsymbol{q},t'}\} \rangle = -i \langle \alpha_{\boldsymbol{q},t} \alpha^*_{\boldsymbol{q},t'} \rangle. \tag{22}$$

While G^R and G^A correspond to response functions to an external excitation, the Keldysh Green's function contains information on the system's correlations. In particular, it gives access to the quasiparticle momentum distribution via the relation

$$iG^K_{\boldsymbol{q},t,t} = 2n_{\boldsymbol{q},t} + 1, \tag{23}$$

deduced from Eq. (12). The description of the anomalous distribution $m_{\boldsymbol{q},t}$ requires to introduce a corresponding anomalous Keldysh Green's function and is postponed to Sec. III D for clarity.

In the absence of phonon interactions, the Green's functions reduce to their bare values $G^{0,R}$, $G^{0,A}$, $G^{0,K}$ and follow from Gaussian integrations on the quadratic action (17). This allows us to identify the elements of the matrix kernel (18) as

$$[\mathbf{G}^0]^{-1} = \begin{pmatrix} 0 & [G^{0,A}]^{-1} \\ [G^{0,R}]^{-1} & -[G^{0,R}]^{-1} \circ G^{0,K} \circ [G^{0,A}]^{-1} \end{pmatrix}, \tag{24}$$

and, correspondingly,

$$\mathbf{G}^0 = \begin{pmatrix} G^{0,K} & G^{0,R} \\ G^{0,A} & 0 \end{pmatrix}. \tag{25}$$

In Eq. (24), the symbol $\circ$ denotes a convolution in the time coordinates. In momentum-time representation, the bare retarded, advanced, and Keldysh Green's functions take the explicit expressions

$$G^{0,R}_{\boldsymbol{q},t,t'} = -i\Theta(t - t') e^{-i\epsilon_q (t - t')}, \tag{26}$$

$$G^{0,A}_{\boldsymbol{q},t,t'} = i\Theta(t' - t) e^{-i\epsilon_q (t - t')}, \tag{27}$$

$$G^{0,K}_{\boldsymbol{q},t,t'} = -i(2n_{\boldsymbol{q},0} + 1) e^{-i\epsilon_q (t - t')}. \tag{28}$$

In the presence of phonon interactions, the inverse of the Green's matrix takes the form

$$[\mathbf{G}]^{-1}_{\boldsymbol{q},t,t'} = \begin{pmatrix} 0 & [G^{0,A}]^{-1} - \Sigma^A \\ [G^{0,R}]^{-1} - \Sigma^R & -\Sigma^K \end{pmatrix}_{\boldsymbol{q},t,t'}. \tag{29}$$

This structure generalizes Eq. (24) by including finite self-energies $\Sigma^{R,A,K}$ that encapsulate the effect of interactions. The self-energies can be computed from perturbation theory with the action (19), a task that will be undertaken in the next section. Comparing Eq. (29) with the definition of $\mathbf{G}$, of the same triangular form as (25), we infer the following Dyson

equations:

$$[G^R]^{-1} = [G^{0,R}]^{-1} - \Sigma^R, \tag{30}$$

$$[G^A]^{-1} = [G^{0,A}]^{-1} - \Sigma^A, \tag{31}$$

$$G^K = G^R \circ \Sigma^K \circ G^A. \tag{32}$$

Within this formalism, the computation of response and correlation functions thus essentially amounts to evaluating the self-energies $\Sigma^{R,A,K}$ at a certain level of approximation.

While the retarded and advanced Green's functions are both Hermitian, $(G^R)^\dagger = G^R$ and $(G^A)^\dagger = G^A$, the Keldysh Green's function is anti-Hermitian, $(G^K)^\dagger = -G^K$ (with the Hermitian conjugate obtained by taking the complex conjugate and reversing time indices). This allows us to parametrize G^K as

$$G^K = G^R \circ F - F \circ G^A, \tag{33}$$

where the Hermitian distribution function F will be related to the phonon momentum distribution below. Combining Eqs. (32) and (33), we infer

$$\Sigma^K = F \circ [G^A]^{-1} - [G^R]^{-1} \circ F, \tag{34}$$

which, by virtue of the Dyson equations (30) and (31), becomes

$$F \circ [G^{0,A}]^{-1} - [G^{0,R}]^{-1} \circ F = \Sigma^K - (\Sigma^R \circ F - F \circ \Sigma^A).$$

Direct evaluation of the left-hand side leads to the following quantum kinetic equation for the distribution function in real-time representation:

$$i(\partial_t + \partial_{t'})F_{\boldsymbol{q},t,t'} = -\Sigma^K_{\boldsymbol{q},t,t'} + (\Sigma^R \circ F - F \circ \Sigma^A)_{\boldsymbol{q},t,t'}. \tag{35}$$

An evaluation of this evolution equation requires the knowledge of the Keldysh and retarded self-energies, which will be both computed in Sec. III C. Before that, we introduce an important assumption that will bring about a first important simplification of Eq. (35).

B. Separation of timescales and on-shell approximation

Two-time nonequilibrium functions such as $F_{\boldsymbol{q},t,t'}$ are most conveniently expressed using the Wigner coordinates $\tau \equiv (t + t')/2$ and $\Delta t \equiv t - t'$. The Wigner transform of a given two-time function $X_{t,t'}$ is defined as $X_{\omega,\tau} = \int d\Delta t\, e^{i\Delta t\omega} X_{\tau+\Delta t/2,\tau-\Delta t/2}$. In the present context, the central time τ is associated with the slow relaxation of the phonons, while the time difference Δt is related to their fast, coherent dynamics [58].

In the presence of interactions, Bogoliubov quasiparticles acquire a finite lifetime $\tau_{\boldsymbol{q}} \sim -1/\mathrm{Im}\Sigma^R_{\boldsymbol{q}}$. As long as interactions are weak, this lifetime is typically very long compared to the coherent timescale $1/\epsilon_{\boldsymbol{q}}$:

$$\tau_{\boldsymbol{q}} \sim -1/\mathrm{Im}\Sigma^R_{\boldsymbol{q}} \gg 1/\epsilon_{\boldsymbol{q}}. \tag{36}$$

This condition, which we will verify *a posteriori* below, also implies that quasiparticles remain well defined during of the out-of-equilibrium evolution. In the limit (36), it can be shown that the Wigner transform of a time convolution reduces [at leading order in $1/(\epsilon_{\boldsymbol{q}}\tau_{\boldsymbol{q}}) \ll 1$] to the product of Wigner transforms [57]. The Wigner transform of Eq. (35) thus simplifies to

$$i\partial_\tau F_{\boldsymbol{q},\omega,\tau} \simeq -\Sigma^K_{\boldsymbol{q},\omega,\tau} + 2iF_{\boldsymbol{q},\omega,\tau}\mathrm{Im}\big(\Sigma^R_{\boldsymbol{q},\omega,\tau}\big). \tag{37}$$

Within the separation of timescales (36), application of the Wigner transform to Eq. (33) also yields

$$iG^K_{\boldsymbol{q},\omega,\tau} \simeq F_{\boldsymbol{q},\tau,\omega}A_{\boldsymbol{q},\omega,\tau}, \tag{38}$$

where

$$A_{\boldsymbol{q},\omega,\tau} \equiv -2\,\mathrm{Im}\big(G^R_{\boldsymbol{q},\omega,\tau}\big) = \frac{-2\,\mathrm{Im}\big(\Sigma^R_{\boldsymbol{q},\omega,\tau}\big)}{|\omega - \epsilon_{\boldsymbol{q}} - \Sigma^R_{\boldsymbol{q},\omega,\tau}|^2}. \tag{39}$$

$A_{\boldsymbol{q},\tau,\omega}$ is the spectral function, which gives the probability density that a quasiparticle with energy ω has the dispersion $\epsilon_{\boldsymbol{q}}$ at a time τ after the quench. Under the condition (36) of well-defined quasiparticles, the spectral function is strongly peaked around $\omega = \epsilon_{\boldsymbol{q}}$ [with $A_{\boldsymbol{q},\tau,\omega} \to 2\pi\delta(\omega - \epsilon_{\boldsymbol{q}})$ in the noninteracting limit]. Integrating Eq. (38) over ω then leads to

$$\int \frac{d\omega}{2\pi} iG^K_{\boldsymbol{q},\omega,\tau} \simeq F_{\boldsymbol{q},\epsilon_{\boldsymbol{q}},\tau} = 2n_{\boldsymbol{q},\tau} + 1, \tag{40}$$

where we used Eq. (23) in the last equality. This relation shows that, as long as the separation of timescales (36) holds, the phonon momentum distribution coincides with the distribution function $F_{\boldsymbol{q},\omega,\tau}$ evaluated at $\omega = \epsilon_{\boldsymbol{q}}$, a property known as the on-shell approximation. To evaluate $n_{\boldsymbol{q},\tau}$, it is thus sufficient to solve the on-shell version of the kinetic equation (37). This is achieved by multiplying the latter by the spectral function and integrating over ω, similarly to Eq. (40). The kinetic equation simplifies to

$$\partial_\tau F_{\boldsymbol{q},\tau} \simeq i\Sigma^K_{\boldsymbol{q},\tau} + 2F_{\boldsymbol{q},\tau}\mathrm{Im}\big(\Sigma^R_{\boldsymbol{q},\tau}\big), \tag{41}$$

where we introduced the simpler notations $F_{\boldsymbol{q},\tau} \equiv F_{\boldsymbol{q},\epsilon_{\boldsymbol{q}},\tau}$ and $\Sigma_{\boldsymbol{q},\tau} \equiv \Sigma_{\boldsymbol{q},\epsilon_{\boldsymbol{q}},\tau}$. Together with Eq. (40), Eq. (41) constitutes a quantum kinetic equation for the momentum distribution of the interacting phonons, which can be directly solved once an approximation for the self-energies is provided.

C. Born approximation

We now evaluate the retarded and Keldysh self-energies $\Sigma^R_{\boldsymbol{q},\tau}$ and $\Sigma^K_{\boldsymbol{q},\tau}$ for a 2D, weakly interacting Bose gas using perturbation theory. In practice, this is achieved by expanding $e^{iS_{\mathrm{int}}}$ and truncating the corresponding series at leading order. For a dilute Bose gas, $e^{iS_{\mathrm{int}}}$ can be expanded at first order in the interaction parameter $g\rho_0$ (Born approximation), such that the retarded Green's function is approximated as

$$\begin{aligned} G^R_{\boldsymbol{q},t,t'} &= -i\langle\alpha_{\boldsymbol{q},t}\tilde{\alpha}^*_{\boldsymbol{q},t'}\rangle = -i\int \mathcal{D}[\alpha,\tilde{\alpha}]\alpha_{\boldsymbol{q},t}\tilde{\alpha}^*_{\boldsymbol{q},t'}e^{i(S_0+S_{\mathrm{int}})} \\ &\simeq -i\int \mathcal{D}[\alpha,\tilde{\alpha}]\alpha_{\boldsymbol{q},t}\tilde{\alpha}^*_{\boldsymbol{q},t'}e^{iS_0}\big(1 - S^2_{\mathrm{int}}/2\big). \end{aligned} \tag{42}$$

Comparison with Eq. (30) then provides an explicit expression for the self-energy. The Gaussian integral in Eq. (42) yields three contributions to Σ^R, each appearing with a multiplicity of 8 and represented by the one-loop diagrams in Fig. 1(b)

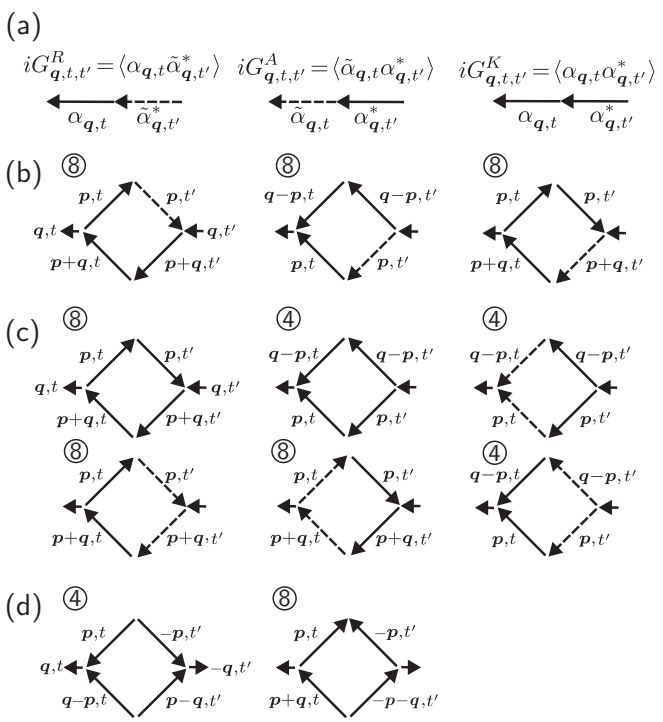

FIG. 1. (a) Diagrammatic conventions for the Green's functions. Dashed (solid) lines refer to a quantum $\tilde{\alpha}$ (classical α) field variable. Arrows are directed from a conjugated field variable to a nonconjugated one. (b) Diagrams contributing to the retarded self-energy Σ^R [Eq. (43)]. Each diagram has multiplicity 8. (c,d) The diagrams contributing to the normal Σ^K and anomalous $\mathscr{S}^K$ Keldysh self-energies, with the corresponding multiplicities indicated.

[see Fig. 1(a) for the diagrammatic conventions]:

$$\Sigma^R_{\boldsymbol{q},t,t'} = 2i \int_{\boldsymbol{p}} \big[\Lambda^2_{\boldsymbol{p},\boldsymbol{q}} G^K_{\boldsymbol{p}+\boldsymbol{q},t,t'} G^{0,A}_{\boldsymbol{p},t',t} + \Lambda^2_{\boldsymbol{p},\boldsymbol{q}-\boldsymbol{p}} G^K_{\boldsymbol{q}-\boldsymbol{p},t,t'} G^{0,R}_{\boldsymbol{p},t,t'} + \Lambda^2_{\boldsymbol{p},\boldsymbol{q}} G^K_{\boldsymbol{p},t',t} G^{0,R}_{\boldsymbol{p}+\boldsymbol{q},t,t'} \big]. \tag{43}$$

In the Wigner representation, this reads

$$\Sigma^R_{\boldsymbol{q},\omega,\tau} = 2i \int_{\boldsymbol{p},\nu} \big\{ \Lambda^2_{\boldsymbol{p},\boldsymbol{q}-\boldsymbol{p}} G^K_{\boldsymbol{p},\nu,\tau} G^{0,R}_{\boldsymbol{q}-\boldsymbol{p},\omega-\nu} + \Lambda^2_{\boldsymbol{p},\boldsymbol{q}} \big[G^K_{\boldsymbol{p},\nu} G^{0,R}_{\boldsymbol{p}+\boldsymbol{q},\omega+\nu} + G^K_{\boldsymbol{p}+\boldsymbol{q},\nu+\omega,\tau} G^{0,A}_{\boldsymbol{p},\nu} \big] \big\}. \tag{44}$$

Next, we use that $G^{0,R}_{\boldsymbol{p},\nu} = -i\pi\delta(\nu - \epsilon_{\boldsymbol{p}})$, $G^{0,A}_{\boldsymbol{p},\nu} = i\pi\delta(\nu - \epsilon_{\boldsymbol{p}})$, and $G^K_{\boldsymbol{p},\tau,\nu} \simeq -2i\pi F_{\boldsymbol{p},\nu,\tau}\delta(\nu - \epsilon_{\boldsymbol{p}})$ [cf. Eqs. (26), (27), and (28)], multiply Eq. (44) by the spectral function $A_{\boldsymbol{q},\omega,\tau}$ and integrate over ω and ν using that $A_{\boldsymbol{q},\omega,\tau}$ is peaked around $\omega \simeq \epsilon_{\boldsymbol{q}}$. This yields the on-shell self-energy

$$\Sigma^R_{\boldsymbol{q},\tau} \simeq -2i\pi \int_{\boldsymbol{p}} \big[\Lambda^2_{\boldsymbol{p},\boldsymbol{q}} (F_{\boldsymbol{p},\tau} - F_{\boldsymbol{p}+\boldsymbol{q},\tau}) \delta(\epsilon_{\boldsymbol{q}} + \epsilon_{\boldsymbol{p}} - \epsilon_{\boldsymbol{p}+\boldsymbol{q}}) + \Lambda^2_{\boldsymbol{p},\boldsymbol{q}-\boldsymbol{p}} F_{\boldsymbol{p},\tau}\, \delta(\epsilon_{\boldsymbol{q}} - \epsilon_{\boldsymbol{p}} - \epsilon_{\boldsymbol{q}-\boldsymbol{p}}) \big]. \tag{45}$$

For a purely phononic dispersion (9), the angular integration in Eq. (45) is divergent, which is a consequence of the resonant character of the cubic interaction (10). In two and three dimensions, this divergence is customarily regularized by taking into account the first nonlinear correction to the Bogoliubov dispersion, $\epsilon_{\boldsymbol{q}} \simeq c|\boldsymbol{q}| + (c\xi^2/2)|\boldsymbol{q}|^3$ [47,51]. Note that in strongly interacting gases in one dimension, it was suggested that the divergence should be instead resolved via a self-consistent Born approximation [9]. In the present case of a dilute Bose gas, however, such an approach would lead to subleading contributions and is therefore *a priori* not adequate. Including the leading-order corrections to the linear dispersion and performing the angular integrations in Eq. (45), we finally obtain

$$\Sigma^R_{\boldsymbol{q},\tau} = -\frac{i}{2} \int_0^\infty d\boldsymbol{p}\, \mathcal{K}^L_{\boldsymbol{p},\boldsymbol{q}} (F_{\boldsymbol{p},\tau} - F_{\boldsymbol{p}+\boldsymbol{q},\tau}) - i \int_0^q d\boldsymbol{p}\, \mathcal{K}^B_{\boldsymbol{p},\boldsymbol{q}} F_{\boldsymbol{q},\tau}, \tag{46}$$

where

$$\mathcal{K}^L_{\boldsymbol{p},\boldsymbol{q}} = \frac{3\sqrt{3}c}{8\pi\rho_0} p(p+q), \quad \mathcal{K}^B_{\boldsymbol{p},\boldsymbol{q}} = \frac{3\sqrt{3}c}{16\pi\rho_0} p(q-p). \tag{47}$$

We now come to the Keldysh self-energy Σ^K, which is calculated perturbatively from the Dyson equation (32). At the Born approximation, this is achieved by approximating the left-hand side by

$$G^K_{\boldsymbol{q},t,t'} \simeq -i \int \mathcal{D}[\alpha]\, \alpha_{\boldsymbol{q},t} \alpha^*_{\boldsymbol{q},t'} e^{iS_0} (1 - S^2_{\rm int}/2). \tag{48}$$

Evaluation of the Gaussian integral involves the six one-loop diagrams represented in Fig. 1(c), which lead to

$$\Sigma^K_{\boldsymbol{q},t,t'} = i \int_{\boldsymbol{p}} \big[2\Lambda^2_{\boldsymbol{p},\boldsymbol{q}} \big(G^K_{\boldsymbol{p}+\boldsymbol{q},t,t'} G^K_{\boldsymbol{p},t',t} + G^{0,A}_{\boldsymbol{p},t',t} G^{0,R}_{\boldsymbol{p}+\boldsymbol{q},t,t'} + G^{0,R}_{\boldsymbol{p},t',t} G^{0,A}_{\boldsymbol{p}+\boldsymbol{q},t,t'} \big) + \Lambda^2_{\boldsymbol{p},\boldsymbol{q}-\boldsymbol{p}} \big(G^K_{\boldsymbol{q}-\boldsymbol{p},t,t'} G^K_{\boldsymbol{p},t,t'} + G^{0,A}_{\boldsymbol{q}-\boldsymbol{p},t,t'} G^{0,A}_{\boldsymbol{p},t,t'} + G^{0,R}_{\boldsymbol{q}-\boldsymbol{p},t,t'} G^{0,R}_{\boldsymbol{p},t,t'} \big) \big]. \tag{49}$$

To evaluate this expression, we proceed as for Σ^R, namely, we move to Wigner representation, multiply Eq. (49) by the spectral function, and integrate over Wigner frequencies. This leads to the on-shell value

$$\Sigma^K_{\boldsymbol{q},\tau} = -2i\pi \int_{\boldsymbol{p}} \big[2\Lambda^2_{\boldsymbol{p},\boldsymbol{q}} (F_{\boldsymbol{p}+\boldsymbol{q}} F_{\boldsymbol{p}} - 1) \delta(\epsilon_{\boldsymbol{q}} + \epsilon_{\boldsymbol{p}} - \epsilon_{\boldsymbol{p}+\boldsymbol{q}}) + \Lambda^2_{\boldsymbol{p},\boldsymbol{q}-\boldsymbol{p}} (F_{\boldsymbol{q}-\boldsymbol{p}} F_{\boldsymbol{p}} + 1) \delta(\epsilon_{\boldsymbol{q}} - \epsilon_{\boldsymbol{p}} - \epsilon_{\boldsymbol{q}-\boldsymbol{p}}) \big]. \tag{50}$$

By finally computing the angular integration using the regularization procedure explained above, we find

$$\Sigma^K_{\boldsymbol{q},\tau} = -i \int_0^\infty d\boldsymbol{p}\, \mathcal{K}^L_{\boldsymbol{p},\boldsymbol{q}} (F_{\boldsymbol{p}+\boldsymbol{q},\tau} F_{\boldsymbol{p},\tau} - 1) - i \int_0^q d\boldsymbol{p}\, \mathcal{K}^B_{\boldsymbol{p},\boldsymbol{q}} (F_{\boldsymbol{q}-\boldsymbol{p},\tau} F_{\boldsymbol{p},\tau} + 1). \tag{51}$$

Equations (46) and (51) constitute the final expressions for the normal self-energies, which once inserted in Eq. (41), provide a kinetic equation for the momentum distribution $n_{\boldsymbol{q},\tau}$. Before coming to that point, however, we now discuss the perturbation theory for the anomalous distribution.

D. Anomalous momentum distribution

To derive a quantum kinetic equation for the anomalous phonon distribution $m_{\boldsymbol{q},\tau}$, one is naturally led to define a Keldysh Green's function from the anomalous anticommutator $\langle\{\hat{a}_{\boldsymbol{q},t}, \hat{a}_{-\boldsymbol{q},t'}\}\rangle$, in analogy with Eq. (22). Such a

definition, however, gives rise to fast temporal oscillations at the scale of $1/\epsilon_{\boldsymbol{q}}$, which are incompatible with the requirement of the timescales separation discussed in Sec. III B. This can be seen at the level of the free-field theory, which yields $\langle\{\hat{a}_{\boldsymbol{q},t}, \hat{a}_{-\boldsymbol{q},t'}\}\rangle = 2\langle\hat{a}_{\boldsymbol{q},0}\hat{a}_{-\boldsymbol{q},0}\rangle \exp(-2i\epsilon_{\boldsymbol{q}}\tau)$, where $\tau = (t+t')/2$. To get rid of these fast variations, we move to the rotating time frame by employing the transformation $\alpha_{\boldsymbol{q},t} \to \alpha_{\boldsymbol{q},t}\exp(i\epsilon_{\boldsymbol{q}}t)$, following [9,10]. In this rotating frame, we can safely define the anomalous Keldysh Green's function as

$$i\mathscr{G}^K_{\boldsymbol{q},t,t'} = \langle\{\hat{a}_{\boldsymbol{q},t}, \hat{a}_{-\boldsymbol{q},t'}\}\rangle = \langle\alpha_{\boldsymbol{q},t}\alpha_{-\boldsymbol{q},t'}\rangle. \tag{52}$$

From its definition (13), the anomalous momentum distribution follows from $2m_{\boldsymbol{q},t} = i\mathscr{G}^K_{\boldsymbol{q},t,t}$ [59]. In the presence of phonon interactions, $\mathscr{G}^K$ acquires a finite (anomalous) self-energy $\mathscr{S}^K$, defined through a Dyson equation similar to Eq. (32):

$$\mathcal{G}^K = G^R \circ \mathscr{S}^K \circ G^A. \tag{53}$$

In the rotating frame, $\mathscr{G}^K$ is also anti-Hermitian, and can therefore be parametrized in a similar way as G^K [see Eq. (33)]:

$$\mathscr{G}^K = G^R \circ \mathscr{F} - \mathscr{F} \circ G^A. \tag{54}$$

Combining the four relations (30), (31), (53), and (54) and making use of the condition of timescales separation, as explained in Sec. III B, we infer the anomalous version of the on-shell kinetic equation (41) as

$$\partial_\tau \mathscr{F}_{\boldsymbol{q},\tau} \simeq i\mathscr{S}^K_{\boldsymbol{q},\tau} + 2\mathscr{F}_{\boldsymbol{q},\tau}\mathrm{Im}\big(\Sigma^R_{\boldsymbol{q},\tau}\big). \tag{55}$$

As compared to Eq. (41), the difference lies in the anomalous Keldysh self-energy $\mathscr{S}^K_{\boldsymbol{q},\tau}$, which can be computed by perturbation theory from Eq. (53). Similarly to the normal correlator, this is done by approximating the left-hand side of Eq. (53) by

$$\mathcal{G}^K_{\boldsymbol{q},t,t'} \simeq -i\int \mathcal{D}[\alpha]\,\alpha_{\boldsymbol{q},t}\alpha_{-\boldsymbol{q},t'}e^{iS_0}\big(1 - S^2_{\mathrm{int}}/2\big). \tag{56}$$

Note that, different from the calculation of Σ^K, here the Wick decomposition following from the Gaussian integral (56) is performed by only considering pairings of anomalous correlators, which is a consequence of the resonant character of the interaction, see [9] for details. This leads to the two self-energy diagrams displayed in Fig. 1(d), which explicitly read as

$$\mathscr{S}^K_{\boldsymbol{q},t,t'} = i\int_{\boldsymbol{p}}\big[2\Lambda^2_{\boldsymbol{p},\boldsymbol{q}}\,\mathscr{G}^K_{\boldsymbol{p}+\boldsymbol{q},t,t'}\mathscr{G}^K_{\boldsymbol{p},t',t} + \Lambda^2_{\boldsymbol{p},\boldsymbol{q}-\boldsymbol{p}}\,\mathscr{G}^K_{\boldsymbol{p},t,t'}\mathscr{G}^K_{\boldsymbol{q}-\boldsymbol{p},t,t'}\big].$$

We then proceed as in Sec. III C, i.e., we compute the Wigner transform of $\mathscr{S}^K_{\boldsymbol{q},t,t'}$, multiply by the spectral function, and integrate over Wigner frequencies. It eventually yields

$$\begin{aligned}\mathscr{S}^K_{\boldsymbol{q},\tau} = &-i\int_0^\infty d\boldsymbol{p}\,\mathcal{K}^L_{\boldsymbol{p},\boldsymbol{q}}\mathscr{F}_{\boldsymbol{p}+\boldsymbol{q},\tau}\mathscr{F}_{\boldsymbol{p},\tau}\\ &- i\int_0^q d\boldsymbol{p}\,\mathcal{K}^B_{\boldsymbol{p},\boldsymbol{q}}\mathscr{F}_{\boldsymbol{q}-\boldsymbol{p},\tau}\mathscr{F}_{\boldsymbol{p},\tau}.\end{aligned} \tag{57}$$

Once inserted in Eq. (55), this provides an explicit expression for the kinetic equation for $m_{\boldsymbol{q},\tau}$.

IV. PHONON QUANTUM KINETICS

A. Kinetic equations

Inserting the expressions (46) and (51) of the normal self-energies into Eq. (41) and using Eq. (40), we obtain the final form of the kinetic equation for the phonon momentum distribution $n_{\boldsymbol{q},\tau}$ at the Born approximation:

$$\begin{aligned}\partial_\tau n_{\boldsymbol{q},\tau} = &\,2\int_0^\infty d\boldsymbol{p}\,\mathcal{K}^L_{\boldsymbol{p},\boldsymbol{q}}[n_{\boldsymbol{p}+\boldsymbol{q}}(n_{\boldsymbol{p}}+n_{\boldsymbol{q}}+1) - n_{\boldsymbol{p}}n_{\boldsymbol{q}}]\\ &+ 2\int_0^q d\boldsymbol{p}\,\mathcal{K}^B_{\boldsymbol{p},\boldsymbol{q}}[n_{\boldsymbol{p}}n_{\boldsymbol{q}-\boldsymbol{p}} - n_{\boldsymbol{q}}(n_{\boldsymbol{p}}+n_{\boldsymbol{q}-\boldsymbol{p}}+1)],\end{aligned} \tag{58}$$

where, for notation simplicity, we dropped the τ indices in the collision integrals and we recall that the kernels $\mathcal{K}^L_{\boldsymbol{p},\boldsymbol{q}}$ and $\mathcal{K}^B_{\boldsymbol{p},\boldsymbol{q}}$ are given by Eq. (47). Note that, alternatively to the present Keldysh approach, such a kinetic equation can also be derived from detailed-balance arguments combined with the Fermi golden rule [50,60,61], or from cumulant theories [22,49].

The only quantity conserved during the time evolution governed by Eq. (58) is the (phononic) energy: $\partial_\tau\int_{\boldsymbol{q}} c|\boldsymbol{q}|n_{\boldsymbol{q},\tau} = 0$ for all τ. The kinetic equation includes two collision integrals, which correspond to the well-known Beliaev (B) and Landau (L) three-particle scattering processes. The Beliaev process describes the splitting $q \to (p, q-p)$ of the probe phonon of momentum q into two phonons of momenta p and $q-p$, while the Landau process describes the recombination $(q,p) \to p+q$ of the probe phonon with another one, each process coming together with its reversed version. Both the Landau and Beliaev processes lead to a relaxation of the momentum distribution toward a thermal equilibrium at long time,

$$n_{\boldsymbol{q},\tau\to\infty} \equiv n^{\mathrm{th}}_{\boldsymbol{q}} = \frac{1}{\exp(\epsilon_{\boldsymbol{q}}/T)-1}, \tag{59}$$

a solution which cancels both collision integrals in Eq. (58). In the present nonequilibrium scenario, the temperature T characterizes the effective thermal equilibrium reached by the phonon gas a long time after the quench. In practice, this temperature is determined from the law of energy conservation mentioned above. A concrete example of this will be given in Sec. V.

The kinetic equation for the anomalous phonon distribution is similarly derived by inserting Eqs. (46) and (57) into Eq. (55). This gives:

$$\begin{aligned}\partial_\tau m_{\boldsymbol{q},\tau} = &\,2\int_0^\infty d\boldsymbol{p}\,\mathcal{K}^L_{\boldsymbol{p},\boldsymbol{q}}(n_{\boldsymbol{p}+\boldsymbol{q}}m_{\boldsymbol{q}} + m_{\boldsymbol{p}}m_{\boldsymbol{p}+\boldsymbol{q}} - n_{\boldsymbol{p}}m_{\boldsymbol{q}})\\ &+ 2\int_0^q d\boldsymbol{p}\,\mathcal{K}^B_{\boldsymbol{p},\boldsymbol{q}}[m_{\boldsymbol{p}}m_{\boldsymbol{q}-\boldsymbol{p}} - m_{\boldsymbol{q}}(n_{\boldsymbol{p}}+n_{\boldsymbol{q}-\boldsymbol{p}}+1)].\end{aligned} \tag{60}$$

Notice that the dynamics of the anomalous distribution is coupled to the evolution of $n_{\boldsymbol{q},\tau}$. Furthermore, unlike $n_{\boldsymbol{q},\tau}$, the anomalous distribution vanishes at long time,

$$m_{\boldsymbol{q},\tau\to\infty} = 0, \tag{61}$$

a result expected for a quantum gas at thermal equilibrium. At any finite time, however, $m_{\boldsymbol{q},\tau}$ is, in general, nonzero and

may significantly impact the intermediate-time dynamics of physical observables.

B. Near-equilibrium solutions

Before examining the consequences of the phonon relaxation on a concrete scenario, it is useful to discuss the near-equilibrium case, which, for a quench experiment, typically corresponds to the long-time regime where the distributions $m_{\boldsymbol{q},\tau}$ and $n_{\boldsymbol{q},\tau}$ become close to their equilibrium values (59) and (61). To this aim, we substitute $n_{\boldsymbol{q},\tau} = n_{\boldsymbol{q}}^{\rm th} + \delta n_{\boldsymbol{q},\tau}$ with $\delta n_{\boldsymbol{q},\tau} \ll n_{\boldsymbol{q}}^{\rm th}$ in the kinetic equation (58) and linearize. If only the Beliaev collision integral is kept, this leads to

$$\partial_\tau \delta n_{\boldsymbol{q},\tau} \simeq -2\gamma_{\boldsymbol{q}}^B \delta n_{\boldsymbol{q},\tau}, \quad \gamma_{\boldsymbol{q}}^B = \frac{\sqrt{3}c}{32\pi\rho_0} q^3. \tag{62}$$

This describes an exponential relaxation governed by the Beliaev damping rate $\gamma_{\boldsymbol{q}}^B$. Note that, alternatively, the latter could have been directly derived from the self-energy (46) evaluated at equilibrium, $\gamma_{\boldsymbol{q}}^B = -{\rm Im}\Sigma_{\boldsymbol{q}}^R(n_{\boldsymbol{q}}^{\rm th})$. In two dimensions, the Beliaev damping rate (62) was previously derived in [51] using the Matsubara formalism.

If, on the other hand, only the Landau collision integral in Eq. (58) is considered, the linearization procedure provides

$$\partial_\tau \delta n_{\boldsymbol{q},\tau} \simeq -2\gamma_{\boldsymbol{q}}^L \delta n_{\boldsymbol{q},\tau}, \quad \gamma_{\boldsymbol{q}}^L = \frac{\sqrt{3}\pi}{8\rho_0 c} q T^2, \tag{63}$$

which now involves the Landau damping rate $\gamma_{\boldsymbol{q}}^L$ [51]. A comparison of Eqs. (62) and (63) shows that Beliaev processes are mostly effective when the long-time equilibrium temperature vanishes. Landau processes, on the contrary, typically dominate at finite temperature. In the relaxation following a quantum quench, this is the most common situation since the quench inevitably injects a certain amount of energy into the system, eventually leading to a finite-temperature state at long time.

A near-equilibrium expansion, finally, can also be applied to the anomalous momentum distribution, using that $m_{\boldsymbol{q},\tau} \ll 1$ at long time. Expanding Eq. (60) for small $\delta n_{\boldsymbol{q},\tau}$ and small $m_{\boldsymbol{q},\tau}$ then yields

$$\partial_\tau m_{\boldsymbol{q},\tau} \simeq -2\gamma_{\boldsymbol{q}}^{L,B} m_{\boldsymbol{q},\tau}, \tag{64}$$

depending on which of the Beliaev or Landau processes dominates.

V. APPLICATION: NONEQUILIBRIUM STRUCTURE FACTOR AND COHERENCE

A. Quench protocol

We now apply the above formalism to a concrete scenario. Consider a uniform 2D Bose gas, initially at equilibrium at temperature T_0 in a superfluid state with interaction strength g_0. The initial (prequench) quasiparticle distributions are thus given by

$$n_{\boldsymbol{q}}^0 = \frac{1}{\exp(\epsilon_{\boldsymbol{q}}^0/T_0) - 1}, \quad m_{\boldsymbol{q}}^0 = 0, \tag{65}$$

where $\epsilon_{\boldsymbol{q}}^0 = \sqrt{E_{\boldsymbol{q}}(E_{\boldsymbol{q}} + 2g_0\rho_0)}$, with $E_{\boldsymbol{q}} = \boldsymbol{q}^2/2m$. As a quench protocol, we suppose that around the time $\tau = 0$ the interaction strength is changed from $g_0 > 0$ to another positive value $g \neq g_0$. The simplest description of this problem, studied, e.g., in [42,62], consists in assuming that the interaction change occurs *instantaneously* at $\tau = 0$. In that case, applying the Bogoliubov transformation (6) at both $\tau = 0^-$ and $\tau = 0^+$ and using the continuity of the field operator (2), we obtain the following relation between the postquench $(\hat{a}_{\boldsymbol{q}}^{\rm ps}, \hat{a}_{\boldsymbol{q}}^{\rm ps\dagger})$ and prequench $(\hat{a}_{\boldsymbol{q}}^0, \hat{a}_{\boldsymbol{q}}^{0\dagger})$ Bogoliubov operators:

$$\begin{pmatrix} \hat{a}_{\boldsymbol{q}}^{\rm ps\dagger} \\ \hat{a}_{-\boldsymbol{q}}^{\rm ps} \end{pmatrix} = \frac{1}{2\sqrt{\epsilon_{\boldsymbol{q}}\epsilon_{\boldsymbol{q}}^0}} \begin{pmatrix} \epsilon_{\boldsymbol{q}} + \epsilon_{\boldsymbol{q}}^0 & \epsilon_{\boldsymbol{q}} - \epsilon_{\boldsymbol{q}}^0 \\ \epsilon_{\boldsymbol{q}} - \epsilon_{\boldsymbol{q}}^0 & \epsilon_{\boldsymbol{q}} + \epsilon_{\boldsymbol{q}}^0 \end{pmatrix} \begin{pmatrix} \hat{a}_{\boldsymbol{q}}^{0\dagger} \\ \hat{a}_{-\boldsymbol{q}}^0 \end{pmatrix}.$$

where $\epsilon_{\boldsymbol{q}} = \sqrt{E_{\boldsymbol{q}}(E_{\boldsymbol{q}} + 2g\rho_0)}$. The postquench normal and anomalous momentum distributions then take the form

$$n_{\boldsymbol{q}}^{\rm ps} = n_{\boldsymbol{q}}^0\big(2d_{\boldsymbol{q}}^2 + 1\big) + d_{\boldsymbol{q}}^2, \tag{66}$$

$$m_{\boldsymbol{q}}^{\rm ps} = \sqrt{d_{\boldsymbol{q}}^2 + d_{\boldsymbol{q}}^4}\big(2n_{\boldsymbol{q}}^0 + 1\big), \tag{67}$$

with $d_{\boldsymbol{q}} \equiv (\epsilon_{\boldsymbol{q}} - \epsilon_{\boldsymbol{q}}^0)/(2\sqrt{\epsilon_{\boldsymbol{q}}\epsilon_{\boldsymbol{q}}^0})$. At this stage, it is instructive to examine the large-q asymptotics of this postquench solution: for $q\xi \gg 1$, Eq. (66) leads to $n_{\boldsymbol{q}}^{\rm ps} \simeq [m\rho_0(g - g_0)]^2/q^4$. An instantaneous interaction quench thus turns the prequench exponential decay (65) into an algebraic one, provoking a logarithmic divergence of the total energy $\int_{\boldsymbol{q}} \epsilon_{\boldsymbol{q}} n_{\boldsymbol{q}}^{\rm ps}$ of the system after the quench. This underlines the somewhat pathological character of the instantaneous quench for a quantum gas, which needs to be regularized by taking into account the finite duration τ_s of the interaction change. Note that a similar divergence occurs in the problem of Tan's contact in Bose gases, originating from the zero-range character of the contact interaction [50,63].

To overcome the ultraviolet divergence resulting from an instantaneous interaction quench, we rather consider the smooth Wood-Saxon quench $g(\tau) = g + (g_0 - g)/(1 + e^{\tau/\tau_s})$, which was revisited recently in [42] and is sketched in the inset of Fig. 2. For this model, Eqs. (66) and (67) still hold, but $n_{\boldsymbol{q}}^0$ $(m_{\boldsymbol{q}}^0)$ and $n_{\boldsymbol{q}}^{\rm ps}$ $(m_{\boldsymbol{q}}^{\rm ps})$ should now be understood as the normal (anomalous) momentum distributions a long time $|\tau| \gg \tau_s$ before and after the interaction jump, respectively, and $d_{\boldsymbol{q}}^2$ is now given by [42]

$$d_{\boldsymbol{q}}^2 = \frac{\sinh^2\left[\pi\left(\epsilon_{\boldsymbol{q}} - \epsilon_{\boldsymbol{q}}^0\right)\tau_s\right]}{\sinh(2\pi\epsilon_{\boldsymbol{q}}^0\tau_s)\sinh(2\pi\epsilon_{\boldsymbol{q}}\tau_s)}. \tag{68}$$

At low momentum, the postquench momentum distribution obeys the asymptotic law

$$n_{\boldsymbol{q}}^{\rm ps} \simeq \frac{T_0}{q}\frac{c^2 + c_0^2}{2cc_0^2}, \tag{69}$$

that involves the prequench $c_0 = \sqrt{g_0\rho_0/m}$ and postquench $c = \sqrt{g\rho_0/m}$ speeds of sound. At large momentum, on the other hand, we have

$$n_{\boldsymbol{q}}^{\rm ps} \propto \exp(-2\pi\tau_s\boldsymbol{q}^2/m). \tag{70}$$

This asymptotic law is similar to that to the prequench thermal distribution, $n_{\boldsymbol{q}}^0 \sim \exp[-\boldsymbol{q}^2/(2mT_0)]$, except that the inverse of the quench duration $1/\tau_s$ now plays the role of the prequench equilibrium temperature.

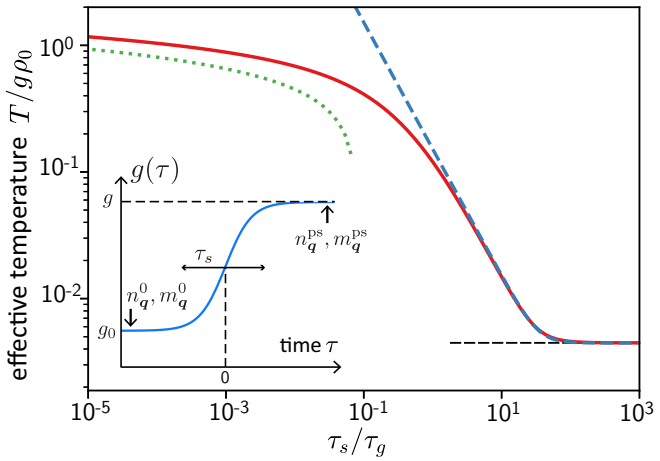

FIG. 2. Inset: Sketch of the Wood-Saxon function modeling an interaction quench of finite duration, with the asymptotic limits $g(-\infty) = g_0$ and $g(\infty) = g$. Main panel: Effective equilibrium temperature reached by the Bose gas a long time after the quench as a function of the quench duration τ_s [expressed in units of $\tau_g \equiv 1/(g\rho_0)$]. The dotted and dashed curves show the asymptotic limits of the temperature for fast and slow quenches, Eqs. (74) and (75), respectively. Parameters are set to $g_0\rho_0 = 0.1$, $g\rho_0 = 0.5$, $T_0/(g_0\rho_0) = 0.01$, $\rho_0\xi^2 = 0.5$.

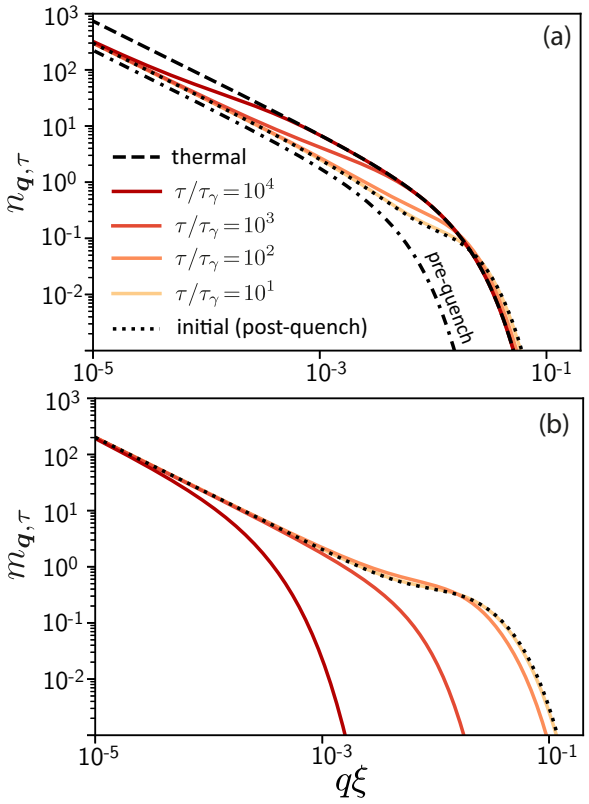

FIG. 3. Time evolution of the phonon (a) normal $n_{q,\tau}$ and (b) anomalous $m_{q,\tau}$ momentum distributions following an interaction quench $g_0 \to g$ near $\tau = 0$. Here we set $g_0\rho_0 = 0.1$, $g\rho_0 = 0.5$, $\rho_0\xi^2 = 0.5$, $\tau_s/\tau_g = 10$, and $T_0/g\rho_0 = 0.01$. The dashed-dotted curve shows the prequench thermal law (65), while dotted curves are the postquench distributions computed from Eqs. (66) and (67), used as initial conditions for the kinetic equations. At long time, $n_{q,\tau}$ converges to the thermal distribution (59) (dashed curve), with an equilibrium temperature well approximated by Eq. (75).

B. Momentum distributions and thermalization

Using the postquench distributions (66) and (67) as initial conditions, we performed numerical simulations of the kinetic equations (58) and (60). The resulting distributions $n_{q,\tau}$ and $m_{q,\tau}$ are shown in Fig. 3 for different times. As expected, we find that $n_{q,\tau}$ slowly evolves toward a thermal distribution of the form (59) at long time. Similarly, $m_{q,\tau}$ converges to zero, with the region where $m_{q,\tau}$ is nonzero shrinking to smaller and smaller q values as time grows. For these simulations, we use as the unit time the Landau relaxation time (63) evaluated at the healing length $\xi = \sqrt{1/(4g\rho_0 m)}$:

$$\tau_\gamma \equiv \frac{1}{2\gamma^L_{q=1/\xi}} = \frac{8}{\sqrt{3}\pi}\rho_0\xi^2\frac{g\rho_0}{T^2}. \tag{71}$$

In order for the kinetic approach presented in Sec. III to be valid, the separation of timescales (36) should be verified, namely, τ_γ should be large compared to the fast timescale $\tau_g \sim 1/(c|\boldsymbol{q}|)$ that governs the coherent dynamics of the Bogoliubov phonons. Evaluated at $q = 1/\xi$, τ_g defines a "nonlinear time" that is sometimes used as a timescale in experiments:

$$\tau_g \sim \frac{\xi}{c} \sim \frac{1}{g\rho_0} \ll \tau_\gamma. \tag{72}$$

From the definition (71) of τ_γ, we find that, in practice, this inequality holds as long as the long-time equilibrium temperature is low enough, precisely when the product $(\rho_0\xi^2)(g\rho_0/T)^2 \gg 1$.

C. Equilibrium temperature

The thermal distribution (59) reached at long time $\tau \gg \tau_\gamma$ is represented by the dashed curve in Fig. 3(a). The associated equilibrium temperature T is entirely determined from energy conservation during the time evolution:

$$\int_{\boldsymbol{q}} \frac{c|\boldsymbol{q}|}{\exp(c|\boldsymbol{q}|/T) - 1} = \frac{\zeta(3)T^3}{\pi\rho_0 c^2} = \int_{\boldsymbol{q}} \epsilon_{\boldsymbol{q}} n^{\rm ps}_{\boldsymbol{q}}. \tag{73}$$

The temperature T, computed from this relation using Eqs. (66) and (68), is displayed in Fig. 2 as a function of the quench duration τ_s. As intuition suggests, T decreases when τ_s increases, i.e., as the quench is more and more adiabatic. The temperature admits a simple expression in the asymptotic regimes $\tau_s \gg \tau_g$ (slow quench) and $\tau_s \ll \tau_g$ (fast quench). For the fast quench we find

$$T \sim \sqrt{\frac{3(g-g_0)^2\rho_0^2}{\pi^2}\ln\left[\sqrt{\frac{\tau_g}{4\pi\tau_s}}\right]}, \quad \tau_s/\tau_g \ll 1, \tag{74}$$

while, for the slow quench,

$$T \simeq \left[\left(\frac{cT_0}{c_0}\right)^3 + \frac{\pi(c-c_0)^2}{2^9\zeta(3)c_0 c\tau_s^3}\right]^{1/3}, \quad \tau_s/\tau_g \gg 1. \tag{75}$$

Both Eqs. (74) and (75) are shown in Fig. 2, together with the exact result. The temperature is minimal for infinitely slow quenches $\tau_s/\tau_g \to \infty$, reaching $T \to (c/c_0)T_0$. As a remark,

the curve in Fig. 2 also indicates that when τ_s is of the order of τ_g or larger, the equilibrium temperature is such that $T \ll g\rho_0$. In this limit, the quasiparticles typically belong to the phononic branch of the dispersion and, at the same time, the condition of separation of timescales is well satisfied. For this reason, in all subsequent numerical simulations, we choose $\tau_s = 10\tau_g$.

D. Nonequilibrium structure factor

To illustrate the concrete impact of the phonon relaxation dynamics in a 2D quenched superfluid, we now study a specific observable, the nonequilibrium quantum structure factor $S_{\boldsymbol{q},\tau} \equiv \langle \delta\hat{\rho}_{\boldsymbol{q},\tau}\delta\hat{\rho}_{-\boldsymbol{q},\tau}\rangle$. The structure factor is the Fourier transform of the spatial density-density correlator of the superfluid. This quantity was recently measured experimentally, in an ultracold Bose gas in two dimensions [31] and in a quantum fluid of light produced in a hot atomic vapor [39], both experiments involving a quench of the interaction strength. In practice, the nonequilibrium structure factor provides a simple observable to characterize the dynamical emergence of interference between quasiparticles emitted at the quench, which manifest themselves as oscillations of $S_{\boldsymbol{q},\tau}$ in space and time. Such oscillations, observed in laboratory superfluids, spark interest because they are analogous to the famous Sakharov oscillations, a characteristic feature in the anisotropy of the cosmic microwave background radiation related to the emission of acoustic waves in the early universe [64]. Employing the Bogoliubov transformations (6) and (7), we can rewrite the structure factor as

$$\begin{aligned} S_{\boldsymbol{q},\tau} &= \frac{E_{\boldsymbol{q}}}{\epsilon_{\boldsymbol{q}}}[2\langle \hat{a}^\dagger_{\boldsymbol{q},\tau}\hat{a}_{\boldsymbol{q},\tau}\rangle + 1 + 2\,\mathrm{Re}\,\langle \hat{a}_{\boldsymbol{q},\tau}\hat{a}_{-\boldsymbol{q},\tau}\rangle] \\ &= \frac{E_{\boldsymbol{q}}}{\epsilon_{\boldsymbol{q}}}[2n_{\boldsymbol{q},\tau} + 1 + 2\cos(2\epsilon_{\boldsymbol{q}}\tau)m_{\boldsymbol{q},\tau}], \end{aligned} \tag{76}$$

where, in the second equality, we introduced the normal and anomalous phonon distributions. The structure factor primarily exhibits a fast, coherent dynamics described by the term $\propto \cos(2\epsilon_{\boldsymbol{q}}\tau)$. These oscillations stem from the interference between Bogoliubov quasiparticles with momenta $\boldsymbol{q}$ and $-\boldsymbol{q}$ emitted at the quench. On top of these oscillations, $S_{\boldsymbol{q},\tau}$ is characterized by a slow relaxation dynamics due to the quasiparticle interactions that make $n_{\boldsymbol{q},\tau}$ and $m_{\boldsymbol{q},\tau}$ slowly vary in time.

The structure factor is shown in Fig. 4(a) for increasing times, from its postquench to its long-time (thermal) value. Shortly after the quench, $S_{\boldsymbol{q},\tau}$ exhibits sizable oscillations of period $\pi/(c\tau)$ in momentum space. In this regime [up to $\sim 10^2\tau_\gamma$ in Fig. 4(a)], the dynamics is almost purely coherent, $m_{\boldsymbol{q},\tau}$ and $n_{\boldsymbol{q},\tau}$ remaining close to their initial, postquench values. Within this short-time window, which was the main focus of previous experiments [31,39], we can therefore approximate $m_{\boldsymbol{q},\tau} \simeq m^{\mathrm{ps}}_{\boldsymbol{q}}$ and $n_{\boldsymbol{q},\tau} \simeq n^{\mathrm{ps}}_{\boldsymbol{q}}$ in Eq. (76), so that

$$S_{\boldsymbol{q},\tau} \simeq \frac{E_{\boldsymbol{q}}}{\epsilon_{\boldsymbol{q}}}\coth\left(\frac{\epsilon^0_{\boldsymbol{q}}}{2T_0}\right)\left[2d^2_{\boldsymbol{q}} + 1 + 2\sqrt{d^2_{\boldsymbol{q}} + d^4_{\boldsymbol{q}}}\cos(2\epsilon_{\boldsymbol{q}}\tau)\right], \tag{77}$$

which is nothing but the prediction of Bogoliubov perturbation theory. The approximation (77) is shown in Fig. 4(a) at both times $\tau = 10^2\tau_\gamma$ and $10^3\tau_\gamma$. While in the first case it well captures the dynamics, in the second case it is clearly inaccurate. Indeed, at long time quasiparticle interactions become prominent and lead to a damping of the coherent oscillations. Eventually, the latter completely disappear when the system has thermalized, with $S_{\boldsymbol{q},\infty} \simeq (E_{\boldsymbol{q}}/\epsilon_{\boldsymbol{q}})\coth(\epsilon_{\boldsymbol{q}}/2T)$. While a quantitative description of $S_{\boldsymbol{q},\tau}$ at an arbitrary time requires a numerical resolution of the kinetic equations, at long time the phonon distributions can be approximated by their near-equilibrium expressions, obtained from Eqs. (63) and (64). Inserting these solutions into Eq. (77), we find

$$\begin{aligned} S_{\boldsymbol{q},\tau} \simeq{}& \frac{E_{\boldsymbol{q}}}{\epsilon_{\boldsymbol{q}}}\coth\left(\frac{\epsilon_{\boldsymbol{q}}}{2T}\right)(1 - e^{-\gamma_{\boldsymbol{q}}\tau}) \\ &+ \frac{E_{\boldsymbol{q}}}{\epsilon_{\boldsymbol{q}}}\coth\left(\frac{\epsilon^0_{\boldsymbol{q}}}{2T_0}\right)\left[2d^2_{\boldsymbol{q}} + 1 + 2\sqrt{d^2_{\boldsymbol{q}} + d^4_{\boldsymbol{q}}}\cos(2\epsilon_{\boldsymbol{q}}\tau)\right]e^{-\gamma_{\boldsymbol{q}}\tau}, \end{aligned} \tag{78}$$

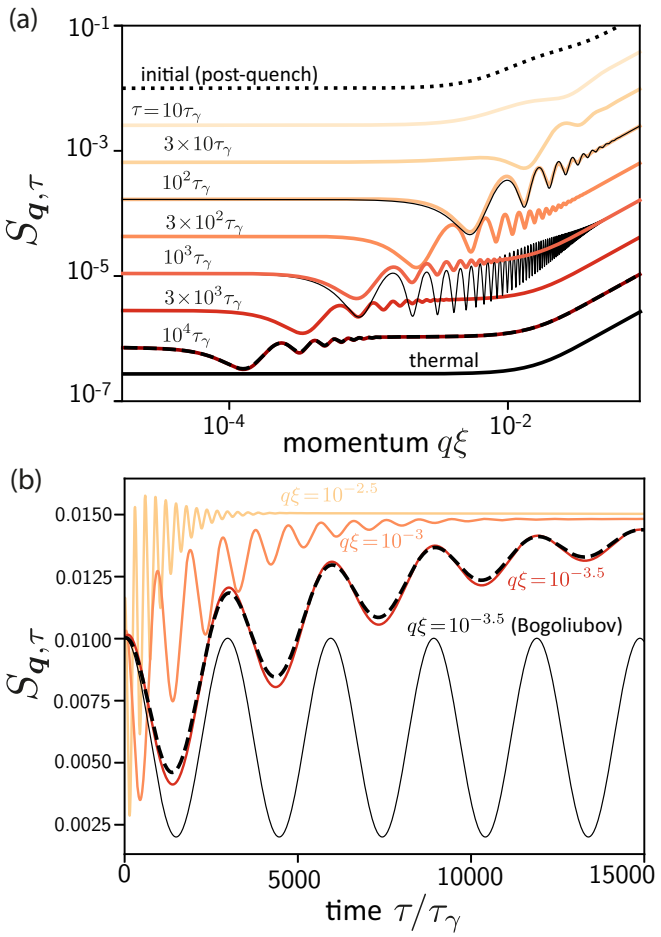

FIG. 4. Nonequilibrium structure factor $S_{\boldsymbol{q},\tau}$, Eq. (76), versus (a) momentum at different times and (b) time at different momenta. For a better readability, in panel (a) the curves are shifted downward as time increases (except $S_{\boldsymbol{q},\tau=0}$, black dotted curve). In both panels, the thin black curves are the Bogoliubov prediction (77), while the dashed curves are the long-time approximation (78). Observe that the Bogoliubov result becomes clearly inaccurate as time increases. Parameters have the same values as in Fig. 3: $g_0\rho_0 = 0.1$, $g\rho_0 = 0.5$, $\rho_0\xi^2 = 5\times10^{-4}$, $\tau_s/\tau_g = 10$, and $T_0/g\rho_0 = 0.01$.

where $\gamma_{\boldsymbol{q}}$ coincides with either the Beliaev (62) or Landau (63) scattering rates depending on the range of momenta probed. In Fig. 4(a), Eq. (78) is superimposed onto the exact result for $\tau = 10^4\tau_\gamma$, using $\gamma_{\boldsymbol{q}} = \gamma_{\boldsymbol{q}}^L$. The agreement is very good in the entire range of q (for the chosen parameters, we have typically $cq \ll T$, such that $\gamma_{\boldsymbol{q}}^L$ is always much larger than $\gamma_{\boldsymbol{q}}^B$).

The impact of the relaxation dynamics of the phonons is seen even more dramatically in Fig. 4(b), which shows the structure factor at fixed momentum as a function of time. In the absence of phonon interactions (Bogoliubov approximation), $S_{\boldsymbol{q},\tau}$ oscillates harmonically. Compared with the exact behavior for $q\xi = 10^{-3.5}$ shows how poor the Bogoliubov approximation becomes as time grows.

E. Nonequilibrium coherence function

As a second illustration, we study the time evolution of the coherence function of the Bose gas consecutive to an interaction quench $g_0 \to g$:

$$G_1(r,\tau) \equiv \langle \hat{\psi}^\dagger(0,\tau)\hat{\psi}(\boldsymbol{r},\tau)\rangle. \tag{79}$$

In the density-phase representation (2), the coherence function can be expressed in terms of the variance of phase and density fluctuations [27]:

$$G_1(r,\tau) = \rho_0 \exp\left\{-\frac{1}{2}\langle :[\hat{\theta}(0,\tau) - \hat{\theta}(\boldsymbol{r},\tau)]^2: \rangle - \frac{1}{8\rho_0}\langle :[\delta\hat{\rho}(0,\tau) - \delta\hat{\rho}(\boldsymbol{r},\tau)]^2: \rangle\right\}, \tag{80}$$

where the : symbol refers to the normal ordering of operators in position representation. Notice that G_1 only depends $r = |\boldsymbol{r}|$ due to rotation invariance. In 2D Bose gases, the spatial dependence of this function is typically dominated by the spatial growth of phase fluctuations, eventually leading to an algebraic decay of G_1. This behavior is noticeably different from the one of 3D Bose gases whose phase fluctuations are very small at low temperature. Using the Bogoliubov transformations (6) and (7) and definitions (12) and (13), we find that Eq. (80) can be rewritten as

$$G_1(r,\tau)/\rho_0 = \mathcal{G}_1(r) g_1(r,\tau). \tag{81}$$

Here

$$g_1(r,\tau) = \exp\left\{-\int_{\boldsymbol{q}} \frac{1}{2}[1-\cos(\boldsymbol{q}\cdot\Delta\boldsymbol{r})]\left[\left(\frac{\epsilon_{\boldsymbol{q}}}{E_{\boldsymbol{q}}} + \frac{E_{\boldsymbol{q}}}{\epsilon_{\boldsymbol{q}}}\right) n_{\boldsymbol{q},\tau} + \left(\frac{E_{\boldsymbol{q}}}{\epsilon_{\boldsymbol{q}}} - \frac{\epsilon_{\boldsymbol{q}}}{E_{\boldsymbol{q}}}\right) m_{\boldsymbol{q},\tau}\cos(2\epsilon_{\boldsymbol{q}}\tau)\right]\right\} \tag{82}$$

encodes the time evolution of the coherence following the quench. The function $\mathcal{G}_1(r)$ is, in contrast, independent of time. It satisfies $\mathcal{G}_1(0) = 1$ and quickly decays to $\mathcal{G}_1(r \gg \xi) \simeq 1 - 1/(16\pi\rho_0\xi^2)$ at distances larger than the healing length, a value that coincides with the quantum depletion of zero-temperature Bose gases in two dimensions. Note that $\mathcal{G}_1$ purely originates from the noncommutation of the Bogoliubov operators involved in Eq. (80) and, as such, would be absent within a classical-field description.

From now on we focus our attention on $g_1(r,\tau)$, which we computed from Eq. (82), using the numerical solutions of the quantum kinetic equations (58) and (60) for $n_{\boldsymbol{q},\tau}$ and $m_{\boldsymbol{q},\tau}$.

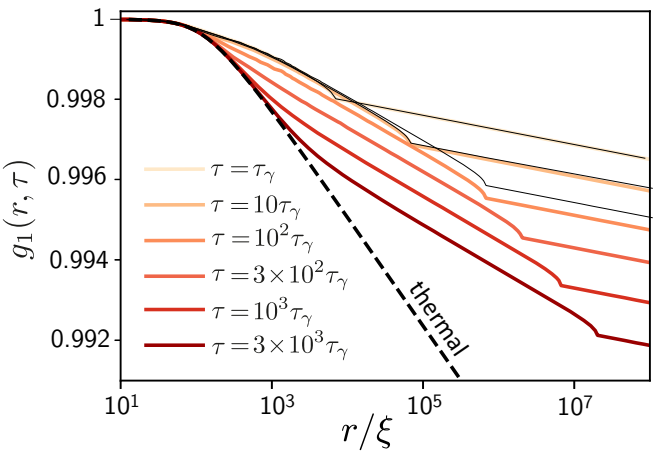

FIG. 5. Nonequilibrium coherence function $g_1(r,\tau)$ versus position r at different times, computed from Eq. (82) together with the numerical solution of quantum kinetic equations for $n_{\boldsymbol{q},\tau}$ and $m_{\boldsymbol{q},\tau}$. The three thin black curves are the Bogoliubov prediction at times $\tau = \tau_\gamma$, $10\tau_\gamma$, and $100\tau_\gamma$. Observe that at $\tau = 100\tau_\gamma$ the Bogoliubov prediction is no longer accurate. The dashed curve shows the long-time, thermal asymptotic value. Parameters are set to $g_0\rho_0 = 0.1$, $g\rho_0 = 0.5$, $\rho_0\xi^2 = 0.5$, $\tau_s/\tau_g = 10$, and $T_0/g\rho_0 = 0.01$.

The full time evolution of this function is shown in Fig. 5 for $g > g_0$, and reveals the successive emergence of three characteristic regimes of algebraic decay. At very short times, first, g_1 mainly exhibits the algebraic decay of the prequench equilibrium state:

$$g_1(r,\tau) \sim \left(\frac{\lambda_0}{r}\right)^{\frac{1}{\rho_0\lambda_0^2}}, \tag{83}$$

with $\lambda_0 = \sqrt{2\pi/(mT_0)}$ the thermal de Broglie wavelength at the (prequench) temperature T_0. Shortly after the quench, then, a second algebraic law emerges at intermediate scales, typically within a light cone of radius $r = 2ct$. This characteristic decay can be described at the level of the Bogoliubov approximation, namely, by simply replacing $n_{\boldsymbol{q},\tau}$ and $m_{\boldsymbol{q},\tau}$ by their postquench values in Eq. (82). This leads to the "prethermal" algebraic law

$$g_1(r,\tau) = \left(\frac{\lambda_0}{r}\right)^{\frac{1+g/g_0}{2\rho_0\lambda_0^2}}. \tag{84}$$

At long time, finally, a third thermal algebraic scaling arises from short scales and eventually extends to all scales as the system fully thermalizes with $n_{\boldsymbol{q},\tau} \to [\exp(cq/T)-1]^{-1}$ and $m_{\boldsymbol{q},\tau} \to 0$:

$$g_1(r,\tau\to\infty) = \left(\frac{\lambda}{r}\right)^{\frac{1}{\rho_0\lambda^2}}, \tag{85}$$

with the algebraic exponent now controlled by the thermal wavelength $\lambda = \sqrt{2\pi/(mT)}$. Note that, in the case $g > g_0$ considered here, the three algebraic exponents satisfy the inequalities

$$\frac{1}{\rho_0\lambda_0^2} \leqslant \frac{1+g/g_0}{2\rho_0\lambda_0^2} \leqslant \frac{1}{\rho_0\lambda^2}, \tag{86}$$

with the two bounds being inverted in the case of a down-quench $g < g_0$. It is instructive, additionally, to compare the exact shape of the coherence function with its Bogoliubov approximation, shown in Fig. 5 for the three shortest times $\tau = \tau_\gamma, 10\tau_\gamma$ and $100\tau_\gamma$. Again, while this approximation is acceptable at short times, it becomes clearly inaccurate starting from $\tau \sim 100\tau_\gamma$. This confirms that in 2D Bose gases, a description in terms of independent quasiparticles should be systematically questioned when dealing with nonequilibrium scenarios.

It is worthwhile to note that, as a low-energy framework, our approach requires the Bose gas to remain in a superfluid state during the dynamical evolution. In particular, the final equilibrium temperature should be well below the critical Kosterlitz-Thouless temperature or, equivalently, the algebraic exponent in Eq. (85) should be much smaller that the critical value $1/4$ [66]. This leads to the condition $(T/g\rho_0) \ll \rho_0\xi^2$, which, in practice, is achieved for a not too strong quench.

VI. CONCLUSION

We presented a general theoretical framework for the many-body, nonequilibrium dynamics of 2D Bose superfluids following a quantum quench. The approach is based on a low-energy quantum hydrodynamic framework and assumes that the timescales respectively associated with the coherent dynamics of the phonons and with the three-phonon interaction processes are well separated. Under this condition, we were able to describe the full time evolution of the phonon normal and anomalous momentum distributions from the coherent prethermal regime to the final thermalization. As an illustration, we applied this framework to a quantitative calculation of two commonly measured observables, the quantum structure factor and the coherence function of the superfluid following an interaction quench.

More generally, the present framework can be used to evaluate any observable, provided that it can be expressed in terms of phonon distributions. While being a many-body quantum description, it can also be used to describe the classical-field limit, to which recent optical-fluid experiments typically belong [38,39,65]. To this aim, one needs to take the limit of large occupation numbers in the kinetic equations (58) and (60) and replace the Bogoliubov operators by commuting scalar fields when expressing observables in terms of phonon momentum distributions. At the level of the field theory, the classical-field regime is described by dropping the interaction processes involving quantum field variables only [67].

As a low-energy framework, our approach requires the quench to leave the Bose gas in the superfluid phase. While the quench dynamics of 2D Bose gases across the Kosterlitz-Thouless transition was recently studied numerically [28,68,69], a general many-body description of this problem is, to our knowledge, still lacking. In practice, this would require to include the dynamics of transverse excitations (vortices) within a nonequilibrium two-fluid model. Finally, exploring the strong-interaction regime in two dimensions, where corrections to the Beliaev and Landau relaxation rates are expected [70,71], would be another interesting challenge for future work.

ACKNOWLEDGMENTS

This project has received financial support from the Agence Nationale de la Recherche (grant ANR-19-CE30-0028-01 CONFOCAL).

[1] A. Polkovnikov, K. Sengupta, A. Silva, and M. Vengalattore, Colloquium: Nonequilibrium dynamics of closed interacting quantum systems, Rev. Mod. Phys. **83**, 863 (2011).

[2] J. Eisert, M. Friesdorf, and C. Gogolin, Quantum many-body systems out of equilibrium, Nat. Phys. **11**, 124 (2015).

[3] M. Gring, M. Kuhnert, T. Langen, T. Kitagawa, B. Rauer, M. Schreitl, I. Mazets, D. A. Smith, E. Demler, and J. Schmiedmayer, Relaxation and Prethermalization in an Isolated Quantum System, Science **337**, 1318 (2012).

[4] T. Langen, R. Geiger, M. Kuhnert, B. Rauer, and J. Schmiedmayer, Local emergence of thermal correlations in an isolated quantum many-body system, Nat. Phys. **9**, 640 (2013).

[5] T. Kinoshita, T. Wenger, and D. S. Weiss, A Quantum Newton's cradle, Nature (London) **440**, 900 (2006).

[6] S. Trotzky, Y.-A. Chen, A. Flesch, I. P. McCulloch, U. Schollwock, J. Eisert, and I. Bloch, Probing the relaxation towards equilibrium in an isolated strongly correlated one-dimensional Bose gas, Nat. Phys. **8**, 325 (2012).

[7] M. Tavora and A. Mitra, Quench dynamics of one-dimensional bosons, Phys. Rev. B **88**, 115144 (2013).

[8] I. V. Protopopov, D. B. Gutman, and A. D. Mirlin, Relaxation in Luttinger liquids: Bose-Fermi duality, Phys. Rev. B **90**, 125113 (2014).

[9] M. Buchhold and S. Diehl, Kinetic theory for interacting Luttinger liquids, Eur. Phys. J. D **69**, 224 (2015).

[10] M. Buchhold, M. Heyl, and S. Diehl, Prethermalization and thermalization of a quenched interacting Luttinger liquid, Phys. Rev. A **94**, 013601 (2016).

[11] J. Lin, K. A. Matveev, and M. Pustilnik, Thermalization of Acoustic Excitations in a Strongly Interacting One-Dimensional Quantum Liquid, Phys. Rev. Lett. **110**, 016401 (2013).

[12] J.-S. Caux and F. H. L. Essler, Time Evolution of Local Observables After Quenching to an Integrable Model, Phys. Rev. Lett. **110**, 257203 (2013).

[13] I. Bouchoule, J. Dubail, L. Dubois, and S. M. Gangardt, Relaxation of phonons in the Lieb-Liniger gas by dynamical refermionization, Phys. Rev. Lett. **130**, 140401 (2023).

[14] R. Nandkishore and D. A. Huse, Many-body localization and thermalization in quantum statistical mechanics, Annu. Rev. Condens. Matter Phys. **6**, 15 (2015)

[15] F. Alet and N. Laflorencie, Many-body localization: An introduction and selected topics, C. R. Phys. **19**, 498 (2018).

[16] D. A. Abanin, E. Altman, I. Bloch, and M. Serbyn, Many-body localization, thermalization, and entanglement, Rev. Mod. Phys. **91**, 021001 (2019).

[17] C. Eigen, J. A. P. Glidden, R. Lopes, N. Navon, Z. Hadzibabic, and R. P. Smith, Universal Scaling Laws in the Dynamics of a Homogeneous Unitary Bose Gas, Phys. Rev. Lett. **119**, 250404 (2017).

[18] C. Eigen, J. A. P. Glidden, R. Lopes, E. A. Cornell, R. P. Smith, and Z. Hadzibabic, Universal Prethermal Dynamics of Bose Gases Quenched to Unitarity, Nature (London) **563**, 221 (2018).

[19] S. Erne, R. Bücker, T. Gasenzer, J. Berges, and J. Schmiedmayer, Universal dynamics in an isolated one-dimensional Bose gas far from equilibrium, Nature (London) **563**, 225 (2018).

[20] J. A. P. Glidden, C. Eigen, L. H. Dogra, T. A. Hilker, T. P. Smith, and Z. Hadzibabic, Bidirectional dynamic scaling in an isolated Bose gas far from equilibrium, Nat. Phys. **17**, 457 (2021).

[21] A. Griffin, T. Nikuni, and E. Zaremba, *Bose-Condensed Gases at Finite Temperatures* (Cambridge University Press, New York, 2009).

[22] M. Van Regemortel, H. Kurkjian, M. Wouters, and I. Carusotto, Prethermalization to thermalization crossover in a dilute Bose gas following an interaction ramp, Phys. Rev. A **98**, 053612 (2018).

[23] I. Chantesana, A. P. Orioli, M. Wouters, and T. Gasenzer, Kinetic theory of nonthermal fixed points in a Bose gas, Phys. Rev. A **99**, 043620 (2019).

[24] A. N. Mikheev, C.-M. Schmied, and T. Gasenzer, Loew-energy effective theory of nonthermal fixed points in a multicomponent Bose gas, Phys. Rev. A **99**, 063622 (2019).

[25] V. N. Popov, On the theory of the superfluidity of two- and one-dimensional Bose systems, Theor. Math. Phys. **11**, 565 (1972).

[26] V. N. Popov, *Functional Integrals in Quantum Field Theory and Statistical Physics* (Reidel, Boston, 1983).

[27] C. Mora and Y. Castin, Extension of bogoliubov theory to quasicondensates, Phys. Rev. A **67**, 053615 (2003).

[28] P. Comaron, F. Larcher, F. Dalfovo, and N. P. Proukakis, Quench dynamics of an ultracold two-dimensional Bose gas, Phys. Rev. A **100**, 033618 (2019).

[29] J. Beugnon and N. Navon, Exploring the Kibble-Zurek mechanism with homogeneous Bose gases, J. Phys. B: At. Mol. Opt. Phys. **50**, 022002 (2017).

[30] S. Sunami, V. P. Singh, D. Garrick, A. Beregi, A. J. Barker, K. Luksch, E. Bentine, L. Mathey, and C. J. Foot, Universal Scaling of the Dynamic BKT Transition in Quenched 2D Bose Gases, arXiv:2209.13587.

[31] C.-L. Hung, V. Gurarie, and C. Chin, From cosmology to cold atoms: observation of Sakharov oscillations in a quenched atomic superfluid, Science **341**, 1213 (2013).

[32] M. Gałka, P. Christodoulou, M. Gazo, A. Karailiev, N. Dogra, J. Schmitt, and Z. Hadzibabic, Emergence of Isotropy and Dynamic Scaling in 2D Wave Turbulence in a Homogeneous Bose Gas, Phys. Rev. Lett. **129**, 190402 (2022).

[33] I. Carusotto and C. Ciuti, Hot atomic vapors for nonlinear and quantum optics, Rev. Mod. Phys. **85**, 299 (2013).

[34] Q. Glorieux, T. Aladjidi, P. D. Lett, and R. Kaiser, Quantum fluids of light, arXiv:2209.04622.

[35] D. Vocke, T. Roger, F. Marino, E. M. Wright, I. Carusotto, M. Clerici, and D. Faccio, Experimental characterization of nonlocal photon fluids, Optica **2**, 484 (2015).

[36] Q. Fontaine, T. Bienaimé, S. Pigeon, E. Giacobino, A. Bramati, and Q. Glorieux, Observation of the Bogoliubov Dispersion in a Fluid of Light, Phys. Rev. Lett. **121**, 183604 (2018).

[37] N. Šantić, A. Fusaro, S. Salem, J. Garnier, A. Picozzi, and R. Kaiser, Nonequilibrium Precondensation of Classical Waves in Two Dimensions Propagating through Atomic Vapors, Phys. Rev. Lett. **120**, 055301 (2018).

[38] M. Abuzarli, N. Cherroret, T. Bienaimé, and Q. Glorieux, Non-equilibrium pre-thermal states in a two-dimensional photon fluid, Phys. Rev. Lett. **129**, 100602 (2022).

[39] J. Steinhauer, M. Abuzarli, T. Aladjidi, T. Bienaimé, C. Piekarski, W. Liu, E. Giacobino, A. Bramati, and Q. Glorieux, Analogue cosmological particle creation in an ultracold quantum fluid of light, Nat. Commun. **13**, 2890 (2022).

[40] S. S. Natu and E. J. Mueller, Dynamics of correlations in a dilute Bose gas following an interaction quench, Phys. Rev. A **87**, 053607 (2013).

[41] P.-É. Larré, D. Delande, and N. Cherroret, Postquench prethermalization in a disordered quantum fluid of light, Phys. Rev. A **97**, 043805 (2018).

[42] G. I. Martone, P.-E. Larré, A. Fabbri, and N. Pavloff, Momentum distribution and coherence of a weakly interacting Bose gas after a quench, Phys. Rev. A **98**, 063617 (2018).

[43] J. Pietraszewicz, M. Stobińska, and P. Deuar, Correlation evolution in dilute Bose-Einstein condensates after quantum quenches, Phys. Rev. A **99**, 023620 (2019).

[44] T. Scoquart, P.-É. Larré, D. Delande, and N. Cherroret, Weakly interacting disordered Bose gases out of equilibrium: from multiple scattering to superfluidity, Europhys. Lett. **132**, 66001 (2020).

[45] T. Bardon-brun, S. Pigeon, and N. Cherroret, Classical Casimir force from a quasi-condensate of light, Phys. Rev. Res. **2**, 013297 (2020).

[46] S. Beliaev, Energy-spectrum of a non-ideal Bose gas, Sov. Phys. JETP **34**, 199 (1958).

[47] L. P. Pitaevskii and S. Stringari, Landau damping in dilute Bose gases, Phys. Lett. A **235**, 398 (1997).

[48] S. Giorgini, Damping in dilute Bose gases: A mean-field approach, Phys. Rev. A **57**, 2949 (1998).

[49] A. Micheli, and S. Robertson, Phonon decay in one-dimensional atomic Bose quasicondensates via Beliaev-Landau damping, Phys. Rev. B **106**, 214528 (2022).

[50] L. P. Pitaevskii and S. Stringari, *Bose-Einstein Condensation* (Oxford University Press, New York, 2003).

[51] M.-C. Chung and A. B. Bhattacherje, Damping in 2D and 3D dilute Bose gases, New J. Phys. **11**, 123012 (2009).

[52] G. Bighin, L. Salasnich, P. A. Marchetti, and F. Toigo, Beliaev damping of the goldstone mode in atomic fermi superfluids, Phys. Rev. A **92**, 023638 (2015).

[53] A. Altland and B. D. Simons, *Condensed Matter Field Theory* (Cambridge University Press, Cambridge, England, 2010).

[54] A. F. Andreev, The hydrodynamics of two- and one-dimensional liquids, Sov. Phys. JETP **51**, 1038 (1980).

[55] L. V. Keldysh, Diagram technique for nonequilibrium processes, Sov. Phys. JETP **20**, 1018 (1965).

[56] L. M. Sieberer, M. Buchhold, and S. Diehl, Keldysh Field Theory for Driven Open Quantum Systems, Rep. Prog. Phys. **79**, 096001 (2016).

[57] A. Kamenev, *Field Theory of Non-Equilibrium Systems* (Cambridge University Press, Cambridge, England, 2011).

[58] T. D. Honeychurch and D. S. Kosov, Timescale separation solution of the Kadanoff-Baym equations for quantum transport in time-dependent fields, Phys. Rev. B **100**, 245423 (2019).

[59] The quantity $\langle\{\hat{a}_{\boldsymbol{q},t}, \hat{a}_{-\boldsymbol{q},t'}\}\rangle$ is *a priori* a complex number, even after moving to the rotating time frame. However, in the present work we always consider initial states such that $i\mathscr{G}^K_{\boldsymbol{q},t,t}$ is real, cf., e.g., Eq. (67). In the general case, one should define the anomalous Keldysh Green's function as a matrix in Nambu space to ensure the antihermiticity of $\mathscr{G}^K$, as presented in Ref. [9].

[60] E. M. Lifshitz and L. P. Pitaevskii, *Physical Kinetics*, Landau and Lifshitz Course of Theoretical Physics, Vol. 10, (Pergamon, Oxford, 1981), Chap. VII.

[61] A. Sinatra and Y. Castin, Coherence time of a Bose-Einstein condensate, Phys. Rev. A **80**, 033614 (2009).

[62] A. Rançon, C.-L. Hung, C. Chin, and K. Levin, Quench dynamics in Bose-Einstein condensates in the presence of a bath: Theory and experiment, Phys. Rev. A **88**, 031601(R) (2013).

[63] S. Tan, Energetics of a strongly correlated Fermi gas, Ann. Phys. (NY) **323**, 2952 (2008).

[64] D. J. Eisenstein and C. L. Bennet, Cosmic sound waves rule, Phys. Today **61**, 44 (2008)

[65] Q. Glorieux, T. Aladjidi, P. D. Lett, and R. Kaiser, Hot atomic vapors for nonlinear and quantum optics, arXiv:2209.04622.

[66] D. R. Nelson and J. M. Kosterlitz, Universal Jump in the Superfluid Density of Two-Dimensional Superfluids, Phys. Rev. Lett. **39**, 1201 (1977).

[67] J. Berges and T. Gasenzer, Quantum versus classical statistical dynamics of an ultracold Bose gas, Phys. Rev. A **76**, 033604 (2007).

[68] L. Mathey, K. J. Günter, J. Dalibard, and A. Polkovnikov, Dynamic Kosterlitz-Thouless transition in two-dimensional Bose mixtures of ultracold atoms, Phys. Rev. A **95**, 053630 (2017).

[69] T. Scoquart, D. Delande, and N. Cherroret, Dynamical emergence of a Kosterlitz-Thouless transition in a disordered Bose gas following a quench, Phys. Rev. A **106**, L021301 (2022).

[70] A. Sinner, N. Hasselmann, and P. Kopietz, Spectral Function and Quasiparticle Damping of Interacting Bosons in Two Dimensions, Phys. Rev. Lett. **102**, 120601 (2009).

[71] A. Sinner, N. Hasselmann, and P. Kopietz, Functional renormalization-group approach to interacting bosons at zero temperature, Phys. Rev. A **82**, 063632 (2010).